A PRELIMINARY STUDY OF FLOW FIELD ABOUT VIKING LANDER MODEL

by

W. Z. Sadeh* and V. A. Sandborn**

Fluid Dynamics and Diffusion Laboratory
Department of Civil Engineering
College of Engineering
Colorado State University
Fort Collins, Colorado

October 1970

* Associate Professor of Engineering
** Professor of Engineering

CER70-71WZS-VAS-18

ABSTRACT

The velocity field about a 1/8 scaled model of the Viking lander was investigated. Measurements of velocity distributions with the model fully immersed in a boundary layer and partially in a uniform flow were performed. The size and shape of the wake and the model effect on the upstream velocity was evaluated. Various velocity defects were estimated.

ACKNOWLEDGMENT

This work was supported by Martin Marietta Corporation, Denver, Colorado. The assistance of many people in carrying out the measurements is appreciated.

TABLE OF CONTENTS

TABLE OF CONTENTS (Continued)

1. INTRODUCTION

The knowledge of the flow field in the surroundings of the Viking lander is of prime importance in determining the feasibility of the planned meteorological measurement on Mars. The various measuring transducers are deployed by means of a 10 to 12 ft long rotating (over 160°) furlable boom. The reliability of the measurements depends upon the knowledge of the flow conditions around the lander. In the surroundings of the lander the velocity distribution is affected by the interaction between the oncoming wind and the local perturbations caused by the lander. Knowledge of these effects permits to correct the measurements in order to obtain the real flow conditions on Mars.

The lander is located inside the so-called turbulent atmospheric boundary layer on Mars. Only limited information about the atmospheric conditions on Mars is available. In Table 1 the meteorological data on Mars is summarized. Due to the relatively large range of wind speed variation, the knowledge of the interaction between the lander and the oncoming wind is of utmost importance. Undoubtedly, the extent of the lander influence, the extent of the wake and the separation do depend upon the prevailing wind velocity and its direction relative to the lander. In order to estimate this interaction a better knowledge of the Mars turbulent atmospheric boundary layer is necessary. It is, further, important to notice that the local topographic conditions, in the vicinity of the lander location, can affect strongly and drastically the flow pattern. Such local topographic variations of the terrain can change completely the velocity distribution and turbulence characteristics of the flow. As a result, the flow pattern around the lander, the wake and separation conditions can change. The knowledge of the terrain

topography is imperative for carried out adequate simulation studies and, hence, for evaluation of the measurements validity.

The peculiar shape of the lander causes important and strong local disturbances which affect severely the flow pattern, the wake extent and development and flow separation. A sketch of the lander is shown in Fig. 1. The lander sharp corners, its non-aerodynamic configuration and various emerging obstructions, viz., cameras poles, RTG, UHF antenna and, in particular, the S-band antenna, alter strongly the velocity field and the wake. Particularly, local separation and wakes due to the aforestated obstructions can change completely the overall wake and separation. In addition, these various local perturbations generate local upward and downward drafts, which in turn, affect the flow field and the wake. Roughly, a wake extending, both vertically and transversally, up to about 10 to 20% of the lander height is expected. This estimation is based on flow about bodies with sharp edges.

The resulting flow field and velocity distribution depends also upon the relative wind direction with respect to the lander. The local perturbations, the extent of the wake, the separation are determined by the lander position. In particular, the position of the 2.5 ft diameter dish of the S-band antenna is of utmost importance. The effect of this dish on the flow depends upon its position. If horizontally positioned, its effect would be smaller than if vertically located. In the former position, the dish is roughly aligned with the main flow streamlines. On the other hand, when in the vertical position the dish represents a very strong and large obstruction. A strong stagnation flow develops, and, thus, a large local wake and strong vortices do occur. Fortunately, it is expected to use this antenna with the dish horizontal most of the time.

The objective of this study was to investigate the velocity field around the Viking lander. This was to be achieved by using a scaled model in a wind tunnel. The velocity variation for the model located inside a fully developed boundary layer and partially in a uniform flow was investigated. During most of this work the measurements were carried out with the dish horizontal. A preliminary survey with the dish vertical was also conducted. The results of this study, using flow similarity, permit to estimate the flow field under the real flow conditions.

2. EXPERIMENTAL APPARATUS

The experimental aim of investigating the velocity field was achieved by using a 1/8 scaled model of the Viking lander in a wind tunnel. The model including all its important dimensions is shown in Fig. 1. It was supplied by Martin Marietta Corporation. The experiment was carried out in the Fluid Dynamics and Diffusion Laboratory, Colorado State University meteorological wind tunnel. This tunnel is of closed circuit type of a 96 ft long working section and of 6 x 6 ft cross section. A schematic diagram of the wind tunnel is displayed in Fig. 2 which also shows the system of coordinate used and all important dimensions. The model location for both cases, inside the thick and thin boundary layer, respectively, is also shown in this figure. The former position is designated by A whereas the latter by B.

The velocity was measured using a Pitot-static tube. A hemispherical standard probe with an impact orifice 1/32-in diameter was employed. The reading of the Pitot-static probe was monitored by means of an electronic pressure meter of capacitance type (Trans-Sonic, Model 120A).

This is a differential micromanometer with an overall range of 30 mm Hg and a resolution of 0.0001 mm Hg. The output of the manometer was recorded using an x-y plotter (Moseley Co., Model 135).

A survey of the velocity direction in the plane of the flow, i.e., plane xz, was conducted employing a three-hole yaw probe. Its reading was monitored by means of the same instruments as for the Pitot-static probe.

An electrically driven traversing mechanism was utilized for continuous movement of the Pitot-static probe. This carriage permitted fine control of position within 0.05 in. Consequently, it was possible to record continuously the Pitot probe output. A photograph of the test section showing the model is given in Fig. 3.

3. RESULTS

The velocity distribution was measured for the following two cases:

1. Model immersed in a fully developed (or thick) boundary layer. The center of the model base was located 70.25 in from the entrance section. This situation is denoted as station A as shown in Fig. 2.

2. Model partially in uniform and partially in a thin boundary layer. In this case, designated as the thin boundary layer survey and by station B, the model was located 2 ft from the entrance section (see Fig. 2). The measurements were conducted for two model positions, i.e., position 1 and 2, which are shown in Figs. 4 and 5. In position 1 the wide side of the model faced the flow whereas in position 2 the vertex of the model triangular body faced the oncoming flow. For both positions, the antenna's dish was located horizontally and vertically. Most of the study was conducted with the dish horizontal. However, some preliminary measurements were also performed with the dish vertical. The

system of coordinate used in the presentation of the results is portrayed in Figs. 2, 4 and 5. The origin is at the geometrical center of the model base. The latter is a circle of 18 1/8-in diameter.

Measurement of velocity were performed downstream of the model, i.e., at x = 9 1/16-in over a distance of ± 17.5 in in the z-direction. Vertical and horizontal surveys were conducted. The horizontal survey was carried out at selected heights depending upon the velocity change. In addition, the velocity upstream of the model along the geometrical center line was also measured. The code used in presenting the results is summarized in Table 2. In case A, i.e., thick boundary layer, a survey was carried out at relatively low velocity. In this case the velocity at the outer edge of the boundary layer was about 5.5 ft/sec whereas at high velocity it was 33 ft/sec. In the thin boundary layer case, i.e., case B, a velocity of about 30 ft/sec was measured at the outer edge of the boundary layer. The Reynolds number was computed based on the velocity at the outer edge of the boundary layer, i.e., the free stream velocity denoted by $U_{o\infty}$, with the model installed. Due to the model shape is practically very difficult to define a characteristic length. Consequently, the Reynolds number per unit length was computed. However, it seems that the length of the side of the body triangular shape or the hydraulic diameter of the lander can be considered as characteristic length. For sake of comparison the Reynolds number per unit length and the boundary layer thickness for the aforementioned three cases are tabulated below:

Case	$U_{o\infty}$ (ft/sec)	δ (in)	Re/L (ft^{-1})
A-HV	33	21	195,000
A-LV	5.5	15	32,500
B	30	2	178,000

In computing the Reynolds number the value for kinematic viscosity used is $16.88\ 10^{-6} ft^2/sec$. The velocity was computed using the relationship

$$U(ft/sec) = k\sqrt{\Delta h(mm\ Hg)} \quad , \qquad (1)$$

where Δh is the reading of the manometer and k is a coefficient. The value of the latter depends on the ambient pressure and temperature. Its value is recorded on the tables attached to the figures. In carrying out the velocity measurement the Pitot-static tube was aligned parallel to the x-axis.

3.1 Thick Boundary Layer Survey, High Velocity, Dish Horizontal; Case A-HV-DH

As mentioned earlier, the center of the model base was located 70.25 ft from the wind tunnel entrance section (see Fig. 2). The velocity was measured downstream of the lander at $x = 9\ 1/16$-in and upstream of the model along the centerline of the model, i.e., along the x-axis. The vertical velocity traverses at $x = 9\ 1/16$-in were carried out at $z = 0, \pm 3.5, \pm 7, \pm 14$ and ± 17.5 in. The horizontal velocity measurement was performed at selected heights depending upon the lander effect on the flow. The velocity in the clear wind tunnel, i.e., empty test section, denoted by CWT, was used as reference velocity in computing the velocity defect. Furthermore, it was also employed as the normalizing velocity when the normalized defect law, i.e., $1 - \frac{U}{U_o} \frac{U_{o\delta}}{U_\delta}$, was computed.

3.1.1 Clear wind tunnel velocity survey, high velocity, A-HV-CWT - The velocity variation with height in the clear wind tunnel at high velocity at $x = 9\ 1/16$-in and $z = 0, \pm 3.5, \pm 7, \pm 14$ and ± 17.5 in is

shown in Figs. A-HV-CWT-VS. In these figures U_o denotes the velocity in the clear wind tunnel. A boundary layer about 20 to 21 in thick was observed. The maximum height of the model is 9.75 in when the dish is vertical. Hence, the model was fully immersed in the boundary layer.

The velocity variation along 6 isoheights, i.e., at $y = 1, 2, 4, 6, 10$ and 15 in over a distance of 35 in (from $z = 17.5$ in to $z = -17.5$ in) is shown in Fig. A-HV-CWT-HS.

The velocity change with height upstream of the model along the centerline, i.e., in plane $z = 0$, is shown in Figs. A-HV-CWT-US-VS. In this diagram the vertical velocity variation at $x = -9\ 1/16$, $-11\ 1/16$, $-14\ 1/16$ and $-19\ 1/16$-in is portrayed. At other positions the velocity was interpolated as needed.

3.1.2 Model in position 1, high velocity, dish horizontal; A-HV-DH-1 - The velocity change with height at $x = 9\ 1/16$-in and $z = 0$, ± 3.5, ± 7, ± 14 and ± 17.5 is shown in Figs. A-HV-DH-1-VS. The effect of the antenna's dish is clearly discerned at $z = 0$. In addition, the defect law, i.e., $1 - U_1/U_o$, and the normalized defect law, i.e., $1 - \frac{U_1}{U_o}\frac{U_{o\delta}}{U_{1\delta}}$, are also shown in Figs. A-HV-DH-1-VS. In these figures U_o denotes the local clear wind tunnel velocity, U_1 is the local velocity when the model is in position 1, $U_{o\delta}$ is the velocity at the outer edge of the empty wind tunnel boundary layer and $U_{1\delta}$ designates the velocity at the outer edge of the boundary layer with the model in position 1. A boundary layer about 21 in thick was observed.

The model affects the velocity variation up to about a height of 12 in, thus, up to 30% of the maximum height of the lander. Recall that the high of the dish is 9.25 in. It is, further, important to

remark the transversal variation of the wake as determined by the lander shape. This change can be discerned from the vertical variation at various positions. It is in particular observed from the velocity change along isoheights shown in Fig. A-HV-DH-1-HS. In these figures the velocity variation at $y = 1, 2, 4, 5, 6, 10$ and 15 in over a distance of 35 in is portrayed. The wake varies from a width of more than 16 in at $y = 1$ in to about 2 in at $y = 10$ to 12 in. Notice that at $y = 1$ and 2 in over a distance of about 6 in negative values were monitored. In other words, near the ground back flow and probably rather local strong vortices prevail. The maximum half of lateral extent of the wake is about 12.7% of length of the body side. The latter is about 6.3 in. Roughly, in the plane $x = 9\ 1/16$-in. the wake reveals a pear-like shape.

The strongest velocity defect was monitored at $y = 1$, 2 and 4 in. At $y = 6$ in the defect is much smaller. At higher heights the defect oscillates about 0.075 and -0.1 due to the various emerging obstructions.

3.1.3 Model in position 2, high velocity, dish horizontal; A-HV-DH-2 - The results for position 2 are depicted in the Figs. A-HV-DH-2-VS and A-HV-DH-2-HS, respectively. In these figures the velocity is denoted by U_2. Roughly, similar results as for position 1 were obtained. On the other hand, various local effects due to the dish position are clearly disc rned. As anticipated, the velocity is strongly affected at $z = 0$ and ± 3.5 in thus, downstream of the dish. A slightly larger asymmetric wake was observed. For instance, at $y = 2$ the wake extends from $z = -12$ to $z = 10$ in. The vertical extent is similar to that observed in position 1.

3.1.4 Model in position 1, high velocity, dish horizontal, upstream survey; A-HV-DH-1-US - The vertical velocity variation upstream of the model along the x-axis at x = -9 1/16, -11 1/16, -14 1/16 and -19 1/16-in and at x = -7 13/16, -18 1/16 and -25 1/16-in is shown in Figs. A-HV-DH-1-US-VS. The effect of the lander is still discerned at x = -25 1/16-in. This is clearly observed from the variation of the velocity defect and the normalized velocity defect. Vertically, the effect of the lander is observed up to a height of about 15 in, thus, up to 5 in above the model.

The velocity change upstream of the model in plane z = 0 along three isoheights, i.e., at y = 1, 4 and 10 in, is portrayed in Figs. A-HV-DH-1-US-HS. In these figures the effect of the lander is observed up to x = - 25 in. The model perturbation decreases with height. At y = 10 in. the disturbance is smaller than at y = 1 but it still can be distinctly observed. Generally, the lander affects the flow over a distance of more than twice its maximum height (9.25 in.).

3.1.5 Model in position 2, high velocity, dish horizontal, upstream survey; A-HV-DH-2-US - The results for position 2 are portrayed in Figs. A-HV-DH-2-US-VS and A-HV-DH-2-US-HS, respectively. Generally, similar results as for position 1 were obtained. The vertical extent of lander effect is slightly smaller. It stretches up to about 12 to 13 in. whereas in position 1 it extends up to approximately 15 in. Furthermore, the horizontal survey reveals that the velocity defect is smaller in this case. However, the longitudinal extent of the lander perturbation stretches over more than twice its maximum height (9.25 in.). A similar result was obtained in position 1.

3.1.6 Model in position 1, high velocity, dish horizontal, yaw angle survey; A-HV-DH-1-YS - The direction of the velocity was measured at $x = 9\ 1/16$-in at three heights, i.e., at $y = 1$, 4 and 10 in. Recall that the yaw angle is the velocity angle in the plane $y = \text{const.}$ measured with respect to the x-axis. The results are shown in Figs. A-HV-DH-1-YS. The strongest direction change was observed at $z = 0$. At this position the direction changes from 7° at $y = 1$ in through -6° at $y = 4$ in to 5° at $y = 10$ in. At all other positions, i.e., at $z = \pm 7.5$ and ± 14 in, the yaw angles varies consistently from 2° to 6°. Thus, the velocity direction is relatively slightly affected by the lander.

3.2 Thick Boundary Layer Survey, Low Velocity, Dish Horizontal; Case A-LV-DH

An exploratory survey at low velocity was conducted in order to obtain an indication of the Reynolds number effect. The measurements were carried out at a free stream velocity of about 5.5 ft/sec. The Reynolds number per unit length was approximately 32,000 while in the high velocity case it was 195,000. This survey was performed with the model located at station A.

In this case, the velocity change with height was measured only at two stations, viz., at $z = \pm 14$ in., in plane $x = 9\ 1/16$ in for both position 1 and 2. The velocity variation in y-direction for the clear wind tunnel is portrayed in Fig. A-LV-CWT. In Figs. A-LV-DH-1-VS and A-LV-DH-2-VS, the results for position 1 and 2, respectively, are shown. In both cases the velocity distribution is affected by the lander. In position 1 the effect is roughly symmetrical and stretches up to a height of about 15 in, i.e., approximately 5 in above the dish. On the other hand, the lander effect is more pronounced for position 2. The velocity defect is consistently

negative and the body affects the velocity distribution up to more than 10 in above the dish.

The velocity variation along four isoheights, viz., at y = 1, 4, 10 and 15 in, is depicted in Figs. A-LV-DH-1-HS and A-LV-DH-2-HS, respectively, at x = 9 1/16 in. Qualitatively, the wake reveals a similar pear-like shape as for high velocity case. At lower elevations the wake is wider than in the latter case. For instance, at y = 1 in in position 1 the wake is approximately 19 in wide. Furthermore, a certain degree of asymmetry was observed. It extends from z = - 9 to z = +10. Roughly, a similar behavior was discerned for position 2. The "dead water" region is larger in position 1 than in position 2. On the other hand, at higher elevations, the wake for position 2 is wider than in position 1.

Quantitatively, the wake extent is affected by the Reynolds number. Unfortunately, the survey at low velocity was too limited to reach definite conclusions. It seems that a detailed survey is necessary in order to assess the Reynolds number effect.

3.3 Thin Boundary Layer Survey, High Velocity, Dish Horizontal; Case B-HV-DH

In order to evaluate the effect of the boundary layer a survey with the model located in a thin boundary layer and partially in uniform flow was conducted. During this investigation the center of the model base was located 2 ft from the wind tunnel entrance section. At this position a boundary layer about 2 in thick was obtained. Consequently, since the main body of the lander is 3.4 in high, the model was only partially immersed in the boundary layer. Moreover, most of the lander and, in particular, the various obstruction were situated in uniform flow

The Reynolds number per unit length was of the same order of magnitude as for station A. In this case it was about 175,000 whereas in the latter it was 195,000.

The velocity variation for the empty test section is displayed in Figs. B-HV-CWT-VS and B-HV-CWT-HS. The measurements were carried out at the same positions as in case A, i.e., in plane $x = 9\ 1/16$ in at $z = 0$, ± 7, ± 14 and ± 17.5 in.

3.3.1 Model in position 1, high velocity, dish horizontal; B-HV-DH-1 The measured velocity variation with height and along isoheights is shown in Figs. B-HV-DH-1-VS and B-HV-DH-1-HS, respectively. In the former case the velocity was measured in plane $x = 9\ 1/16$-in. at $z = 0$, ± 7, ± 14 and ± 17.5 in. The horizontal traverses were carried out along four isoheights, viz., at $y = 1$, 2, 4 and 10 in in the same plane $x = 9\ 1/16$ in.

The effect of the lander extends over a shorter distance than for the thick boundary layer case. However, it is clearly discerned. For instance, at $z = 0$ the model affects the velocity distribution up to about 6 to 8 in. On the other hand, the velocity defect change is affected up to about 10 in, thus, up to about lander height. The wake reveals roughly a similar shape and lateral extent as for case A. On the other hand, the vertical extent of the wake is smaller than in case A. It stretches only up to about the model height, i.e., up to 10 in, whereas in case A it extends up to 30% above the lander. These differences in the wake are due to oncoming flow. In case A the lander is totally immersed in a shear flow whereas in this case only partially exposed to such a flow.

3.3.2 Model in position 2, high velocity, dish horizontal; B-HV-DH-2 - The results are displayed in Figs. B-HV-DH-2-VS and B-HV-DH-2-HS for the vertical and horizontal survey, respectively. In this case the

vertical extent of the wake is smaller than in position 1. Based on the vertical velocity change its height is approximately 6 in. Similarily, the velocity defect is affected only up to about 8 in. The wake exhibits a similar asymmetrical lateral extent as observed in case A.

3.3.3 Model in position 1, high velocity, dish horizontal, upstream survey; B-HV-DH-1-US - The velocity variation in the y-direction upstream of the model (in plane z = 0) at x = -6 13/16, -9 1/16, -14 1/16 and -19 1/16 was measured. The results are shown in Figs. B-HV-DH-1-US-VS. As expected, the vertical distance affected by the lander is shorter than in case A. The velocity is perturbed by the lander up to a height of about 6 to 7 in. The velocity defect decreases with distance from the body. At y = 1 in, the defect $(1-U_1/U_o)$ is about 0.5 at x =-6 13/16 in whereas at x = -19 1/16 in is only 0.1. However, it is still clearly observed at the latter position. Thus, the longitudinal extent of the model influence stretches up to about twice the model height. Recall that in case A it extended to over more than twice the model height.

3.3.4 Model in position 2, high velocity, dish horizontal, upstream survey; B-HV-DH-2-US - The results are displayed in Figs. B-HV-DH-2-US-VS. In this case, due to carriage interaction with the model, the measurements were carried out at x = -10 1/16, -14 1/16 and -19 1/16 in in the plane z = 0, i.e., along the x-axis. Generally, the results are similar to that obtained in position 1. The lander effect stretches over a slightly shorter distance and the defect is smaller than in position 1. Notice that a similar result was obtained in case A.

3.3.5 Model in positions 1 and 2, low velocity, dish horizontal; B-LV-DH-1 or 2 - The velocity change with height in the thin boundary

layer at low velocity, i.e., U_{o_∞} = 5.5 ft/sec, was measured for both position 1 and 2 at $z = \pm 14$ in in the plane $x = 9\ 1/16$ in. The results are portrayed in Figs. B-LV-DH-1-VS and B-LV-DH-2-VS, respectively. As expected, a slightly larger velocity change was observed in position 2.

3.4 Velocity Defect Thin-Thick Boundary Layer, Position 1 and 2, High Velocity, Dish Horizontal; (A-B)-HV-DH-1 or 2

In order to evaluate the shear flow effect on the velocity distribution the velocity defect based on the thin and thick boundary layer was calculated. This velocity defect is

$$(U_1/U_o)_B - (U_1/U_o)_A \qquad (2)$$

The results at $z = 0, \pm 7, \pm 14$ and ± 17.5 in in plane $x = 9\ 1/16$ in are shown in Figs. (A-B)-HV-DH-1-VS and (A-B)-HV-DH-2-VS. The defect is larger in position 1 than for position 2. In particular, at $z = 0$ the maximum defect is twice larger in position 1 than for position 2. These results can be used to evaluate the effect of the boundary layer on the flow field.

3.5 Thick Boundary Layer Survey, High Velocity, Dish Vertical; Case A-HV-DV

A preliminary survey with the antenna's dish vertical was conducted. The aim of this survey was to assess the effect of the dish position on the flow. Since, in this case, the dish constitutes a much stronger obstruction than when it is horizontally placed larger effects are expected. Practically, the dish generates a rather strong stagnation flow and a relatively large local wake develops. In addition, within this wake large vortices can occur.

The measured velocity change with height at $z = 0, \pm 3.5, \pm 7, \pm 14$ and ± 17.5 in in plane $x = 9\ 1/16$ in. for position 1 is shown in

Figs. A-HV-DV-1-VS. The perturbation caused by the dish is stronger than in the DH case. The velocity distribution is affected up to about 15 in, i.e., up to 5 in above the model. Hence, due to the dish, locally the vertical extent of the wake above the body is up to about 50% of the antenna's height. Furthermore, the defect is larger than in the DH case.

The results along isoheights for position 1 are portrayed in Figs. A-HV-DV-1-HS. It can be observed that the velocity fluctuates drastically. The effect of the body can be clearly discerned up to an elevation of about 15 in. Moreover, the lateral extent of the wake is larger than in case of horizontal dish. Roughly, the wake stretches from about 22 in at $y = 2$ in to 10 in at $y = 15$ in. Also, a certain asymmetry in the wake shape is discerned. It stretches over a larger distance on the negative side. Generally, the wake reveals a pear-like shape in the plane $x = 9\ 1/16$ in.

The velocity variation with height for position 2 is displayed in Figs. A-HV-DV-2-VS. A smaller effect than in position 1 is observed. The wake is more similar to that observed with the dish horizontal. It stretches vertically up to about 12 to 14 in. The velocity change along 5 isoheights for position 2 is shown in Figs. A-HV-DV-2-HS. A smoother variation is observed. The lateral extent of the wake is smaller than for position 1.

The velocity variation upstream of the model in the plane $z = 0$ at $x = -9\ 1/16$, $-14\ 1/16$ and $-19\ 1/16$ for position 1 is portrayed in Figs. A-HV-DV-1-US-VS. The velocity distribution is stronger affected than for the DH case. For instance, at all stations the normalized defect is larger in the former case than in the latter case.

Finally, the change of velocity defect along isoheight for position 1 and 2 between the dish horizontal and vertical is shown in Figs. A-HV-(DH-DV)-1-HS and A-HV-(DH-DV)-2-HS. This velocity defect is

$$1 - \frac{U_{DV}}{U_{DH}} \tag{3}$$

The defect is larger for position 1 than for position 2. This is expected, since a larger wake and more disturbed flow was obtained for position 1 with dish vertical.

4. CONCLUSIONS

The results presented indicate clearly that the flow velocity field about the lander is strongly affected by the latter. A relatively large wake of roughly pear-like shape in the vertical plane was observed. Upstream of the lander its effect is observed over a distance of approximately twice its maximum height. The exact size of the wake and its symmetrical or asymmetrical shape depends upon the position of the lander with respect to the approaching wind and the position of the antenna's dish. The largest and most disturbed wake is obtained when the dish is vertical. The smallest disturbance occurs when the dish is horizontal.

For both lander positions, i.e., position 1 and 2, approximately similar results were obtained. However, in position 1 due to the stagnation flow on the model upwind face a larger wake was observed. The upstream influence is practically the same for both positions, it stretches up to about twice the body height, i.e., up to roughly 20 in. The wake extends vertically up to about 30% of the antenna's height above the lander when the dish is horizontal (case A). On the other hand, when

the dish is vertical it stretches up to about 50% of the antenna's height. Basically, it is recommended to carry on the measurement with the dish horizontal.

Comparison of measurements at high and low velocity indicates that the Reynolds number effect is important. Unfortunately, the low velocity survey was too limited for evaluating this effect.

The survey in the thin boundary layer can be used as an indication of the boundary layer correction. The combined thin-thick velocity defect can be used for this purpose.

Similarly, the combined velocity defect for the dish horizontal vertical can be utilized to assess the dish position influence.

Generally, the velocity deflection, i.e., the yaw angle is relatively small, up to about $\pm 6^{o}$. No measurement of the pitch angle was carried out.

4.1 Suggestions for Future Work

The following topics seem worthy of deeper investigation.

(1) The wake characteristics, its longitudinal extent and its shape.

(2) The upstream velocity field off the center line.

(3) The yaw and pitch angle within the regions of interest.

(4) The effect for the boom of the local topographic conditions in the landing terrain. The lander will be operational for about 90 days. Consequently, it would be desirable to simulate the landing terrain in the wind tunnel in order to evaluate its effect on the flow. The terrain topographic configuration can be adequately scaled based on the data supplied by the lander. Then, such a simulation will permit to

dispatch instructions for the most favorable location of the measuring transducers. This method can be proved to be the most effective for obtaining reliable data. It is strongly recommended to consider the feasibility of such an approach.

Table 1.

METEOROLOGY MEASUREMENT RANGES AND ACCURACIES

MEASUREMENT	RANGE	ABSOLUTE ACCURACY*	RELATIVE ACCURACY*
PRESSURE	1-30 MB	±(0.12 MB + .2% OF READING)	
AMBIENT AIR TEMPERATURE	100°-350°K	±3 K**	±1°K**
WIND SPEED	2-150 M/SEC	±1 MPS OR ±10% OF READING (WHICHEVER IS GREATER)	±5 MPS OR 5% (WHICHEVER IS GREATER)
WIND DIRECTION ***	0-360°	±10° (25-150 MPS), ±20° (5-25 MPS)	
WATER VAPOR	180°-255°K (FROST POINT)	±5°K AT 180°K TO ±2°K AT 210°K AND HIGHER	

* ONE-SIGMA FREE-STREAM DATA DISPLAYED ON EARTH

** BASED ON PRELAUNCH PROTECTIVE COATING CHARACTERISTICS.

*** RELATIVE TO PLANETARY AND LANDER COORDINATES.

Table 2

CODE:

A	-	thick boundary layer
B	-	thin boundary layer
HV	-	high velocity
LV	-	low velocity
CWT	-	clear wind tunnel
DH	-	antenna's dish horizontal
DV	-	antenna's dish vertical
U_o	-	velocity-clear wind tunnel
U_1	-	velocity-position 1
U_2	-	velocity-position 2
1	-	position 1
2	-	position 2
US	-	upstream of the model
VS	-	vertical survey
HS	-	horizontal survey
YS	-	yaw angle survey

TABLE:

-	neg. reading
b	no data available

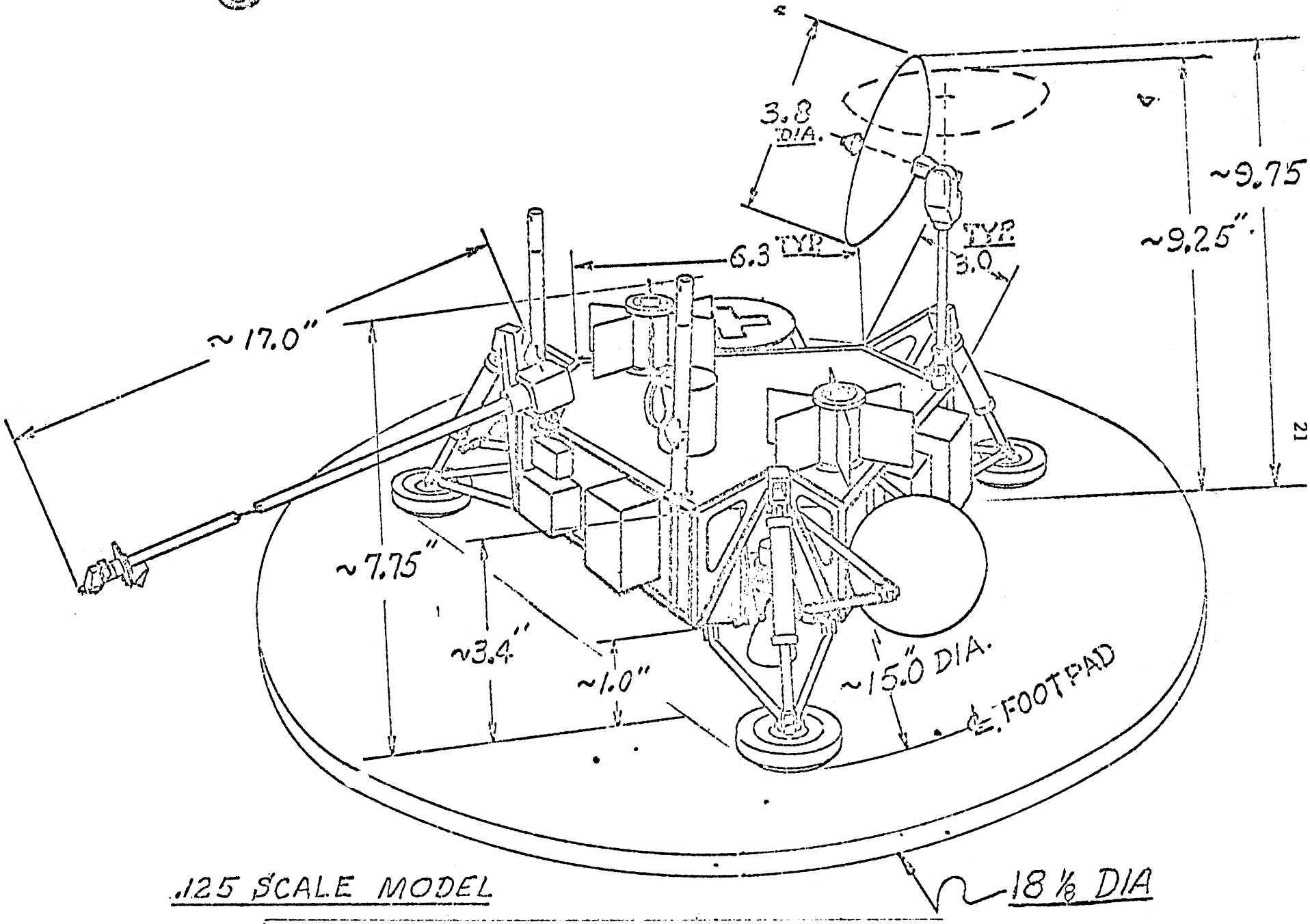

Fig. 1. Sketch of the Viking Lander Model

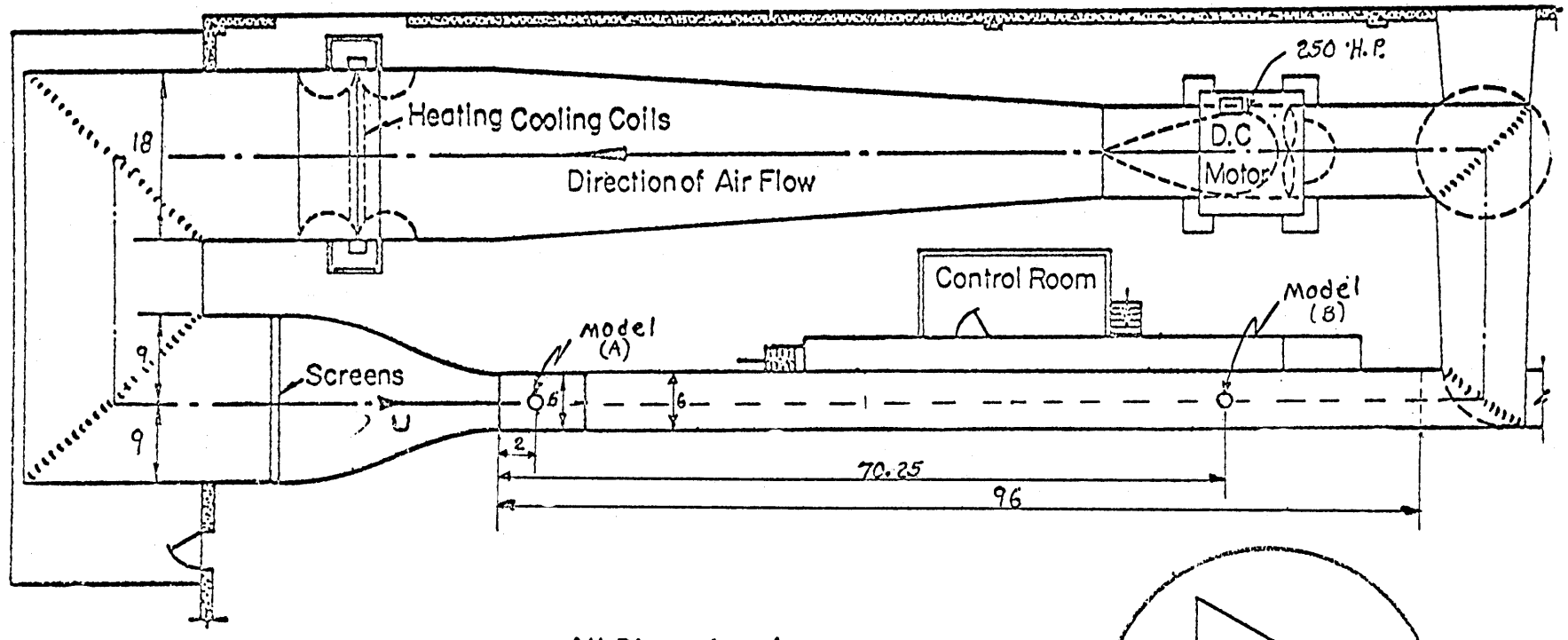

All Dimensions in Feet

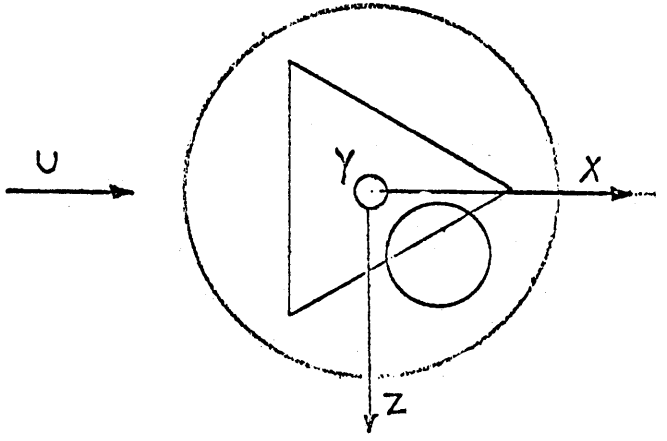

Fig. 2, Sketch of Wind Tunnel.

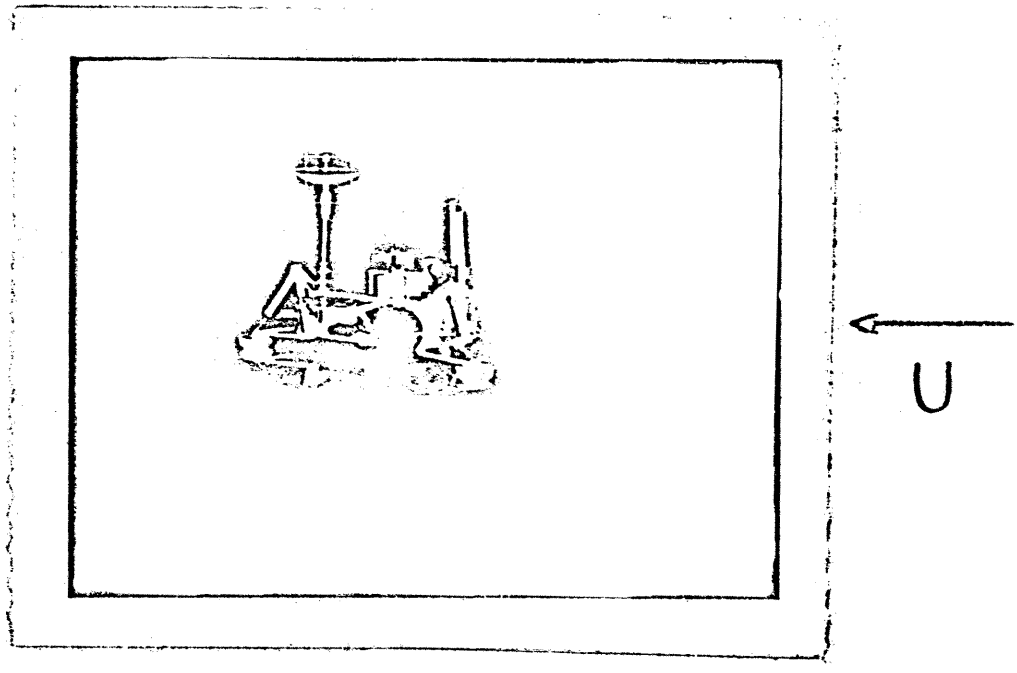

Fig. 3. General view of the model.

POSITION 1

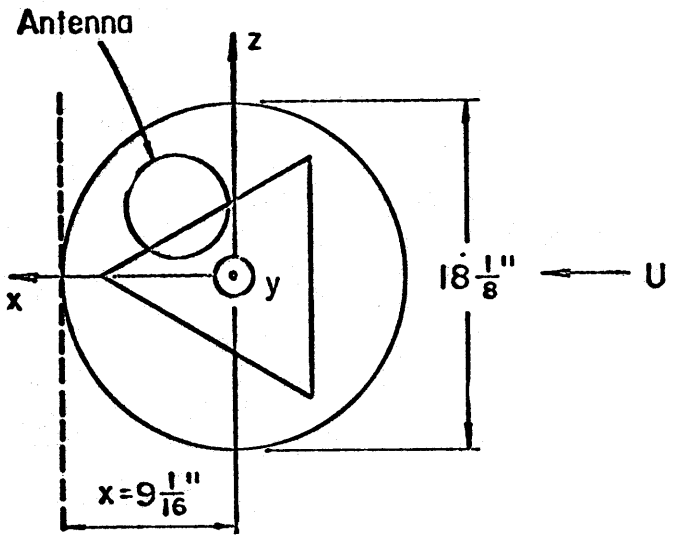

POSITION 2

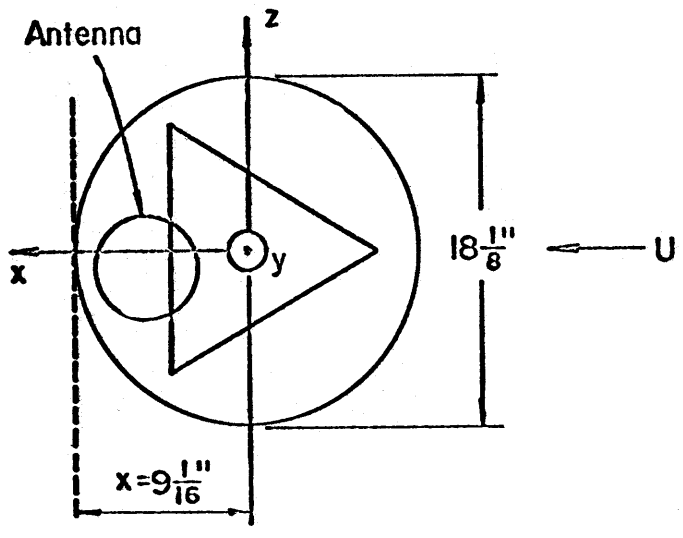

Fig. 4. The model positions with antenna's dish horizontal.

POSITION 1

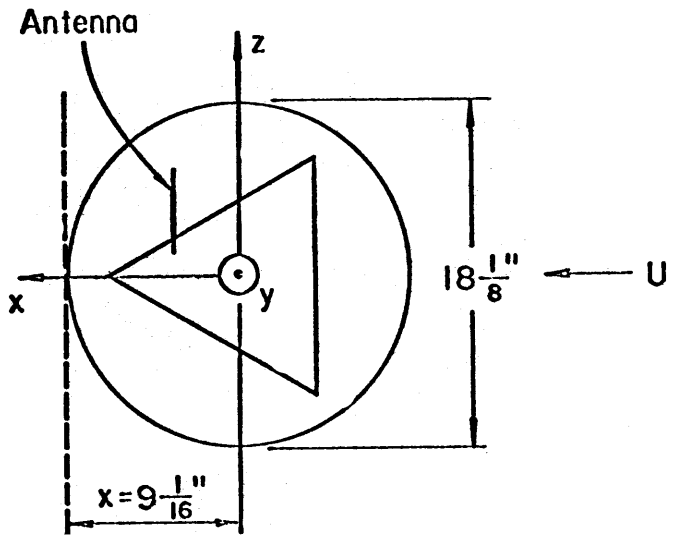

POSITION 2

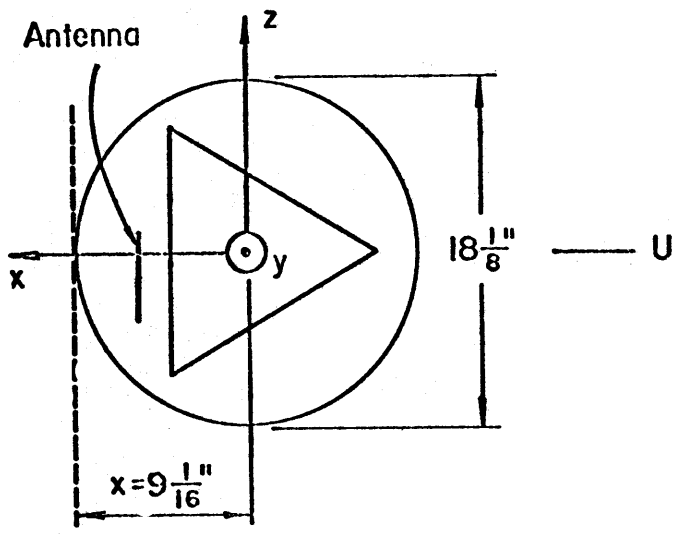

Fig. 5. The model positions with antenna's dish vertical.

APPENDIX A

List of Figures Submitted

The superscript * indicates the last set of measurements

Figure	Description	Position	No. of Figures
A-HV-CWT-VS*	U_o vs. y	z=0,±3.5,±7,±14	2
A-HV-CWT-VS	U_o vs. y	z=0,±7,±14,±17.5	2
A-HV-CWT-HS*	U_o vs. z	y=1,2,4,6,10,15	1
A-HV-CWT-HS	U_o vs. z	y=1,2,4,6,10,15	1
A-HV-CWT-US-VS*	U_o vs. y	x= -9 1/16, -11 1/16, -14 1/16, -19 1/16	1
A-HV-DH-1-VS*	U_1 vs. y	z=0,±3.5,±7,±14	2
A-HV-DH-1-VS*	$1-U_1/U_o$ vs. y	z=0,±3.5,±7,±14	2
A-HV-DH-1-VS*	$1-\frac{U_1}{U_o}\frac{U_{o\delta}}{U_{1\delta}}$ vs. y	z=0,±3.5,±7,±14	2
A-HV-DH-1-VS	U_1 vs. y	z=0,±7,±14,±17.5	2
A-HV-DH-1-VS	U_o-U_1 vs. y	z=0,±7,±14,±17.5	2
A-HV-DH-1-VS	$1-U_1/U_o$ vs. y	z=0,±7,±14,±17.5	2
A-HV-DH-1-HS*	U_1 vs. z	y = 5	1
A-HV-DH-1-HS	U_1 vs. z	y=1,2,4,6,10,15	1
A-HV-DH-1-HS	U_o-U_1 vs. z	y=1,2,4,6,10,15	2
A-HV-DH-1-HS	$1-U_1/U_o$ vs. z	y=1,2,4,6,10,15	2
A-HV-DH-2-VS*	U_2 vs. y	z=0,±3.5,±7,±14	2
A-HV-DH-2-VS*	$1-U_2/U_o$ vs. y	z=0,±3.5,±7,±14	2
A-HV-DH-2-VS*	$1-\frac{U_2}{U_o}\frac{U_{o\delta}}{U_{2\delta}}$ vs. y	z=0,±3.5,±7,±14	2
A-HV-DH-2-VS	U_2 vs. y	z=0,±7,±14,±17.5	2
A-HV-DH-2-VS	U_o-U_2 vs. y	z=0,±7,±14,±17.5	2
A-HV-DH-2-VS	$1-U_2/U_o$ vs. y	z=0,±7,±14,±17.5	2

APPENDIX A - (Continued)

Figure	Description	Position	No. of Figures
A-HV-DH-2-HS*	U_2 vs. z	y=2,5,7.4,9.25	1
A-HV-DH-2-HS	U_2 vs. z	y=1,2,4,6,10,15	1
A-HV-DH-2-HS	U_o-U_2 vs. z	y=1,2,4,6,10,15	2
A-HV-DH-2-HS	$1-U_2/U_o$ vs. z	y=1,2,4,6,10,15	2
A-HV-DH-1-US-VS*	U_1 vs. y	x=-9 1/16,-11 1/16, -14 1/16, -19 1/16	1
A-HV-DH-1-US-VS*	$1-U_1/U_o$ vs. y	x=-9 1/16,-11 1/16, -14 1/16, -19 1/16	1
A-HV-DH-1-US-VS*	$1-\frac{U_1}{U_o}\frac{U_{o\delta}}{U_{1\delta}}$ vs. y	x=-9 1/16,-11 1/16, -14 1/16, -19 1/16	1
A-HV-DH-1-US-VS	U_1 vs. y	x=-7 13/16,-11 1/16, -18 1/16, -25 1/16	1
A-HV-DH-1-US-VS	U_o-U_1 vs. y	x=-7 13/16,-11 1/16, -18 1/16, -25 1/16	1
A-HV-DH-1-US-VS	$1-U_1/U_o$ vs. y	x=-7 13/16,-11 1/16, -18 1/16, -25 1/16	1
A-HV-DH-1-US-HS	U_1 vs. x	y = 1, 4, 10	1
A-HV-DH-1-US-HS	U_o-U_1 vs. x	y = 1, 4, 10	1
A-HV-DH-1-US-HS	$1-U_1/U_o$ vs. x	y = 1, 4, 10	1
A-HV-DH-2-US-VS*	U_2 vs. y	x=-9 1/16,-11 1/16, -14 1/16,-19 1/16	1
A-HV-DH-2-US-VS*	$1-U_2/U_o$ vs. y	x=-9 1/16,-11 1/16, -14 1/16,-19 1/16	1
A-HV-DH-2-US-VS*	$1-\frac{U_2}{U_o}\frac{U_{o\delta}}{U_{2\delta}}$ vs. y	x=-9 1/16,-11 1/16, -14 1/16,-19 1/16	1
A-HV-DH-2-US-VS*	U_2 vs. y	x=-11 1/16,-18 1/16, -25 1/16	1
A-HV-DH-2-US-VS	U_o-U_2 vs. y	x=-11 1/16,-18 1/16, -25 1/16	1
A-HV-DH-2-US-VS	$1-U_2/U_o$ vs. y	x=-11 1/16,-18 1/16, -25 1/16	1

APPENDIX A - (Continued)

Figure	Description	Position	No. of Figures
A-HV-DH-2-US-HS	U_2 vs. x	y = 1, 4, 10	1
A-HV-DH-2-US-HS	U_o-U_2 vs. x	y = 1, 4, 10	1
A-HV-DH-2-US-HS	$1-U_2/U_o$ vs. x	y = 1, 4, 10	1
A-HV-DH-1-YS	α vs. z	y = 1, 4, 10	1
A-HV-DH-1-YS	Vector diagram	y = 1, 4, 10	1
A-LV-CWT-VS	U_o vs. y	z = ±14	1
A-LV-DH-1-VS	U_1 vs. y	z = ±14	1
A-LV-DH-1-VS	U_o-U_1 vs. y	z = ±14	1
A-LV-DH-1-VS	$1-U_1/U_o$ vs. y	z = ±14	1
A-LV-DH-1-HS	U_1 vs. z	y=1,4,10,15	1
A-LV-DH-1-HS	U_o-U_1 vs. z	y=1,4,10,15	1
A-LV-DH-1-HS	$1-U_1/U_o$ vs. z	y=1,4,10,15	1
A-LV-DH-2-VS	U_2 vs. y	z = 14	1
A-LV-DH-2-VS	U_o-U_2 vs. y	z = 14	1
A-LV-DH-2-VS	$1-U_2/U_o$ vs. y	z = 14	1
A-LV-DH-2-HS	U_2 vs. z	y=1,4,10,15	1
A-LV-DH-2-HS	U_o-U_2 vs. z	y=1,4,10,15	1
A-LV-DH-2-HS	$1-U_2/U_o$ vs. z	y=1,4,10,15	1
B-HV-CWT-VS	U_o vs. y	z=0,±7,±14, ±17.5	2
B-HV-CWT-HS	U_o vs. z	y=1,2,4,10	1
B-HV-CWT-US-VS	U_o vs. x	(interpolation)	3
B-HV-DH-1-VS	U_1 vs. y	z=0,±7,±14, ±17.5	2
B-HV-DH-1-VS	U_o-U_1 vs. y	z=0,±7,±14, ±17.5	2
B-HV-DH-1-VS	$1-U_1/U_o$ vs. y	z=0,±7,±14, ±17.5	2

APPENDIX A - (Continued)

Figure	Description	Position	No. of Figures
B-HV-DH-1-HS	U_1 vs. z	y=1,2,4,10	1
B-HV-DH-1-HS	U_o-U_1 vs. z	y=1,2,4,10	1
B-HV-DH-1-HS	$1-U_o/U_1$ vs. z	y=1,2,4,10	1
B-HV-DH-2-VS	U_2 vs. y	z=0,±7,±14, ±17.5	2
B-HV-DH-2-VS	U_o-U_2 vs. y	z=0,±7,±14, ±17.5	2
B-HV-DH-2-VS	$1-U_2/U_o$ vs. y	z=0,±7,±14, ±17.5	2
B-HV-DH-2-HS	U_2 vs. z	y=1,2,4,10	1
B-HV-DH-2-HS	U_o-U_2 vs. z	y=1,2,4,10	1
B-HV-DH-2-HS	$1-U_2/U_o$ vs. z	y=1,2,4,10	1
B-HV-DH-1-US-VS	U_1 vs. y	x=-6 13/16,-9 1/16, -14 1/16,-19 1/16	1
B-HV-DH-1-US-VS	U_o-U_1 vs. y	x=-6 13/16,-9 1/16, -14 1/16,-19 1/16	1
B-HV-DH-1-US-VS	$1-U_1/U_o$ vs. y	x=-6 13/16,-9 1/16, -14 1/16,-19 1/16	1
B-HV-DH-2-US-VS	U_2 vs. y	x=-10 1/16,-14 1/16, -19 1/16	1
B-HV-DH-2-US-VS	U_o-U_2 vs. y	x=-10 1/16,-14 1/16, -19 1/16	1
B-HV-DH-2-US-VS	$1-U_2/U_o$ vs. y	x=-10 1/16,-14 1/16, -19 1/16	1
B-LV-DH-1-VS	U_1 vs. y	z = ±14	1
B-LV-DH-2-VS	U_2 vs. y	z = ±14	1
(A-B)-HV-DH-1-VS	$(U_1/U_o)_B-(U_1/U_o)_A$ vs. y	z=0,±7,±14, ±17.5	2
(A-B)-HV-DH-1-HS	$(U_1/U_o)_B-(U_1/U_o)_A$ vs. z	y= 1,2,4,10	1

APPENDIX A - (Continued)

Figure	Description	Position	No. of Figures
(A-B)-HV-DH-2-VS	$(U_2/U_o)_B-(U_2/U_o)_A$ vs. y	z=0,±7,±14, ±17.5	2
(A-B)-HV-DH-2-HS	$(U_2/U_o)_B-(U_2/U_o{}^0{}_A$ vs. z	y=1,2,4,10	1
A-HV-DV-1-VS*	U_1 vs. y	z=0,±3.5,±7, ±14	2
A-HV-DV-1-VS*	$1-U_1/U_o$ vs. y	z=0,±3.5,±7, ±14	2
A-HV-DV-1-VS*	$1-\frac{U_1}{U_o}\frac{U_{o\delta}}{U_{1\delta}}$ vs. y	z=0,±3.5,±7, ±14	2
A-HV-DV-1-VS	U_1 vs. y	z=0,±7,±14, ±17.5	2
A-HV-DV-1-VS	U_o-U_1 vs. y	z=0,±7,±14, ±17.5	2
A-HV-DV-1-VS	$1-U_1/U_o$ vs. y	z=0,±7,±14, ±17.5	2
A-HV-DV-1-HS*	U_1 vs. z	y=4,5.5,7.5, 9.5	1
A-HV-DV-1-HS	U_1 vs. z	y=2,4,6,10,15	1
A-HV-DV-1-HS	U_o-U_1 vs. z	y=2,4,6,10,15	1
A-HV-DV-1-HS	$1-U_1/U_o$ vs. z	y=2,4,6,10,15	1
A-HV-DV-2-VS	U_2 vs. y	z=7,14,17.5	1
A-HV-DV-2-VS	U_o-U_2 vs. y	z=7,14,17.5	1
A-HV-DV-2-VS	$1-U_2/U_o$ vs. y	z=7,14,17.5	1
A-HV-DV-2-HS	U_2 vs. z	y=2,4,6,10,15	1
A-HV-DV-2-HS	U_o-U_2 vs. z	y=2,4,6,10,15	1
A-HV-DV-2-HS	$1-U_2/U_o$ vs. z	y=2,4,6,10,15	1
A-HV-DV-1-US-VS*	U_1 vs. y	x=-9 1/16,-11 1/16, -14 1/16,-19 1/16	1

APPENDIX A - (Continued)

Figure	Description	Position	No. of Figures
A-HV-DV-1-US-VS*	$1-U_1/U_o$ vs. y	x=-9 1/16,-11 1/16, -14 1/16,-19 1/16	1
A-HV-DV-1-US-VS*	$1-\frac{U_1}{U_o}\frac{U_{o\delta}}{U_{1\delta}}$ vs. y	x=-9 1/16,-11 1/16, -14 1/16,-19 1/16	1
A-HV-DV-1-US-VS	U_1 vs. y	x= -27 1/16	1
A-HV-DV-1-US-VS	U_o-U_1 vs. y	x= -27 1/16	1
A-HV-DV-1-US-VS	$1-U_1/U_o$ vs. y	x= -27 1/16	1
A-HV-(DH-DV)-1-VS	$1-\frac{U_{1DV}}{U_{1DH}}$ vs. y	z=0,±7,±14, ±17.5	2
A-HV-(DH-DV)-1-HS	$1-\frac{U_{1DV}}{U_{1DH}}$ vs. z	y=2,4,6,10,15	1
A-HV-(DH-DV)-2-VS	$1-\frac{U_{2DV}}{U_{2DH}}$ vs. y	z=7,14,17.5	1
A-HV-(DH-DV)-2-HS	$1-\frac{U_{2DV}}{U_{2DH}}$ vs. z	y=2,4,6,10,15	1

In addition to the figures, tables containing the computation and the records of the data were supplied.

Table 1.

METEOROLOGY MEASUREMENT RANGES AND ACCURACIES

MEASUREMENT	RANGE	ABSOLUTE ACCURACY*	RELATIVE ACCURACY*
PRESSURE	1-30 MB	±(0.12 MB + .2% OF READING)	
AMBIENT AIR TEMPERATURE	100°-350°K	±3 K**	±1°K**
WIND SPEED	2-150 M/SEC	±1 MPS OR ±10% OF READING (WHICHEVER IS GREATER)	±5 MPS OR 5% (WHICHEVER IS GREATER)
WIND DIRECTION ***	0-360°	±10° (25-150 MPS), ±20° (5-25 MPS)	
WATER VAPOR	180°-255°K (FROST POINT)	±5°K AT 180°K TO ±2°K AT 210°K AND HIGHER	

* ONE-SIGMA FREE-STREAM DATA DISPLAYED ON EARTH

** BASED ON PRELAUNCH PROTECTIVE COATING CHARACTERISTICS.

*** RELATIVE TO PLANETARY AND LANDER COORDINATES.

Table 2

CODE:

A	-	thick boundary layer
B	-	thin boundary layer
HV	-	high velocity
LV	-	low velocity
CWT	-	clear wind tunnel
DH	-	antenna's dish horizontal
DV	-	antenna's dish vertical
U_o	-	velocity-clear wind tunnel
U_1	-	velocity-position 1
U_2	-	velocity-position 2
1	-	position 1
2	-	position 2
US	-	upstream of the model
VS	-	vertical survey
HS	-	horizontal survey
YS	-	yaw angle survey

TABLE:

-	neg. reading
b	no data available

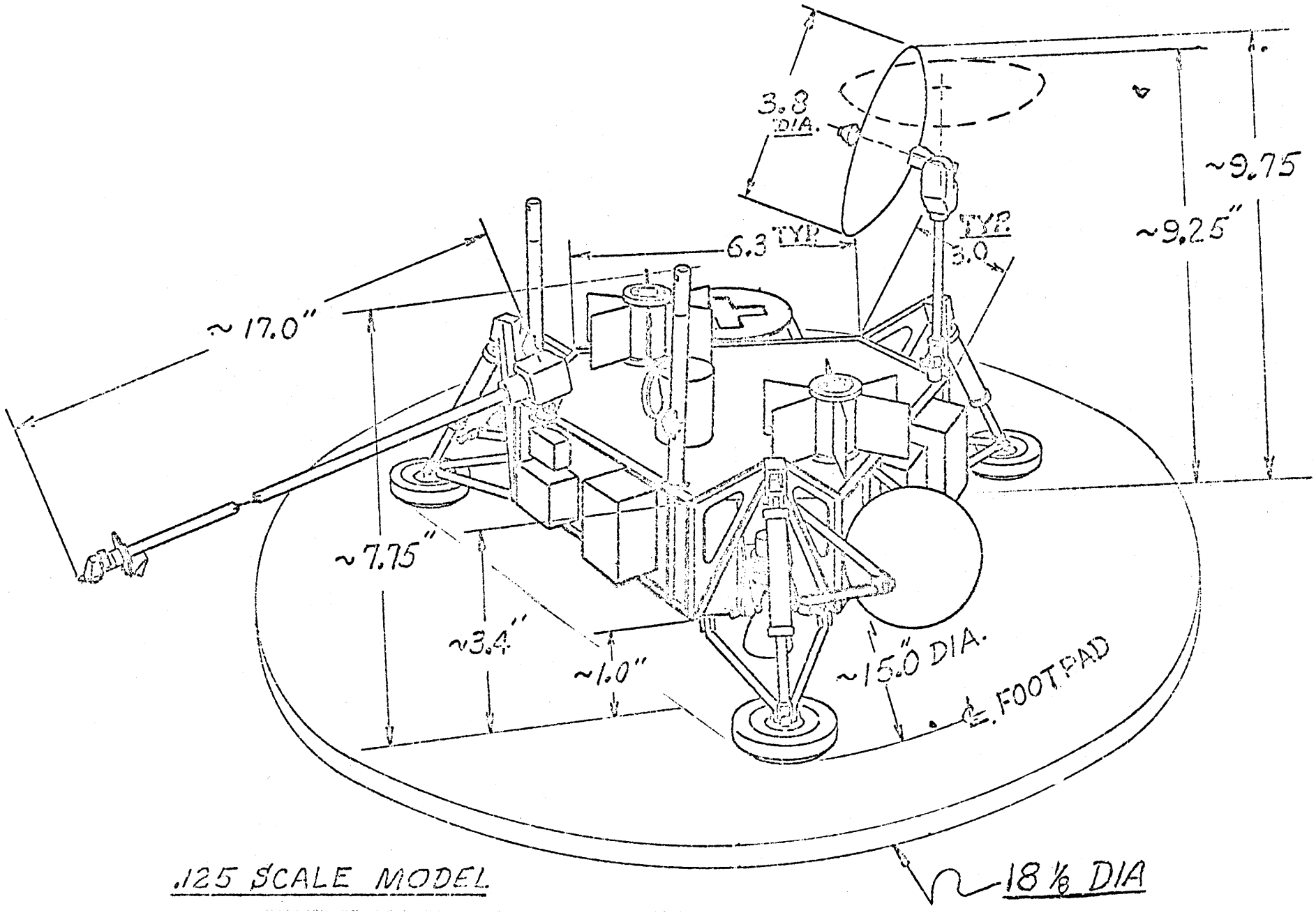

Fig. 1. Sketch of the Viking Lander Model

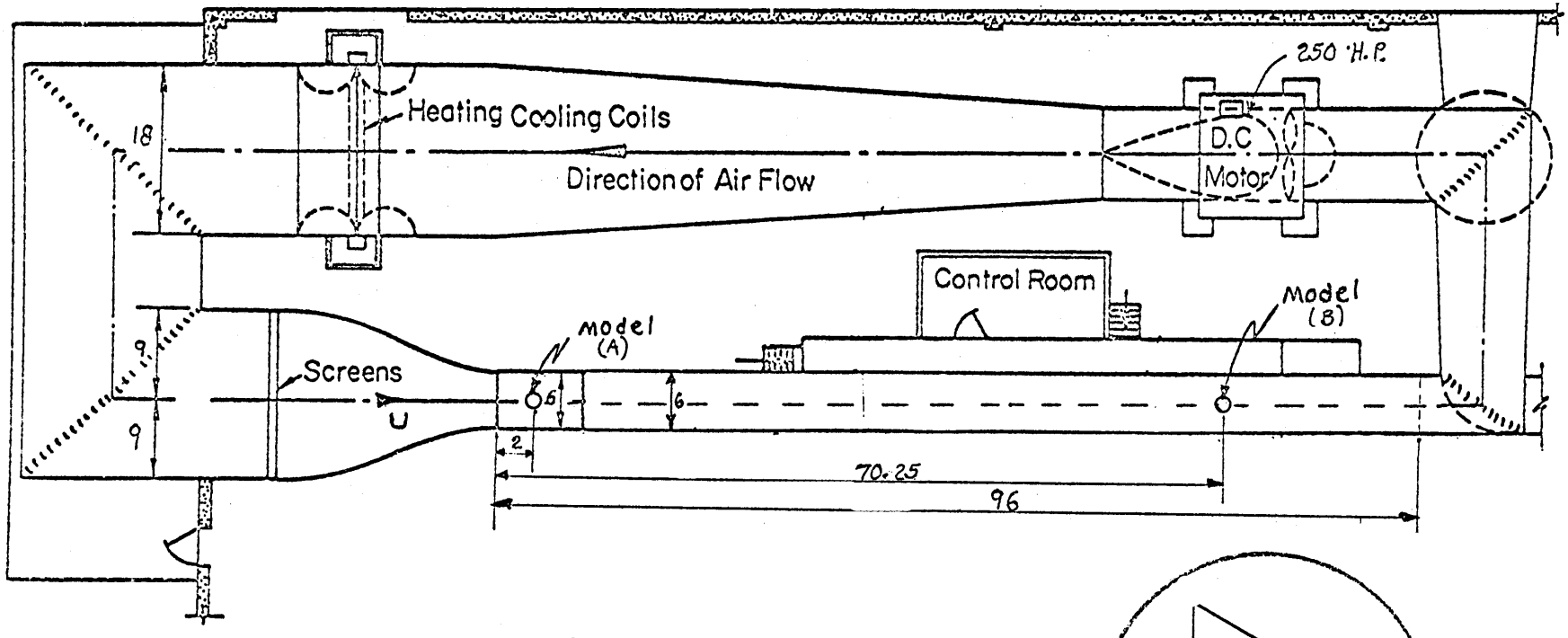

All Dimensions in Feet

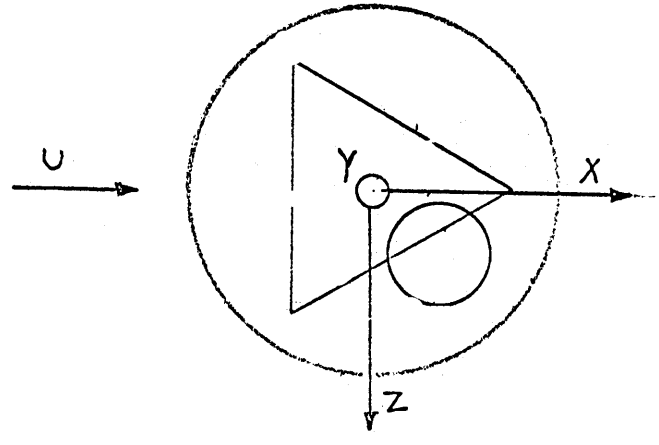

Fig. 2. Sketch of Wind Tunnel.

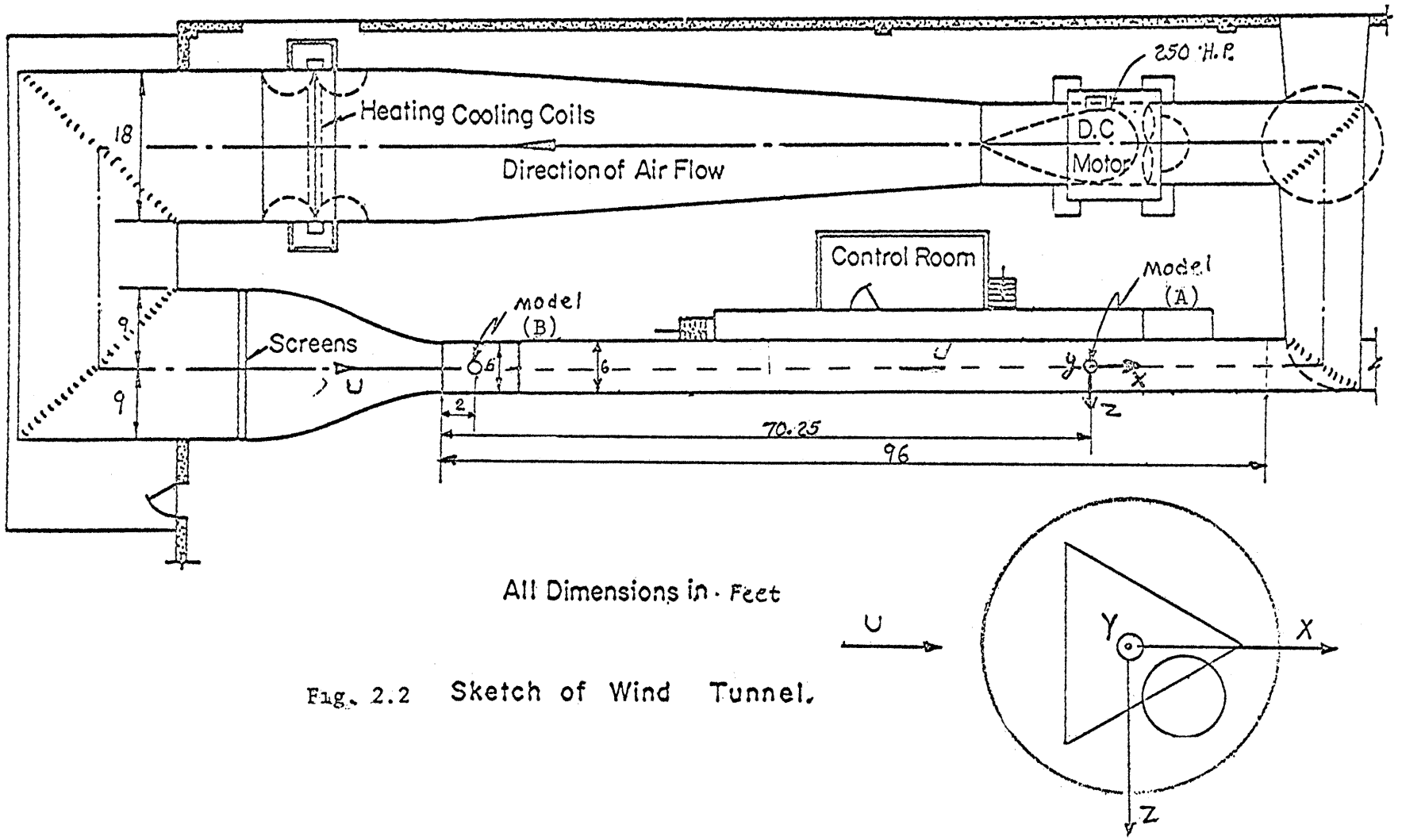

Fig. 2.2 Sketch of Wind Tunnel.

POSITION 1

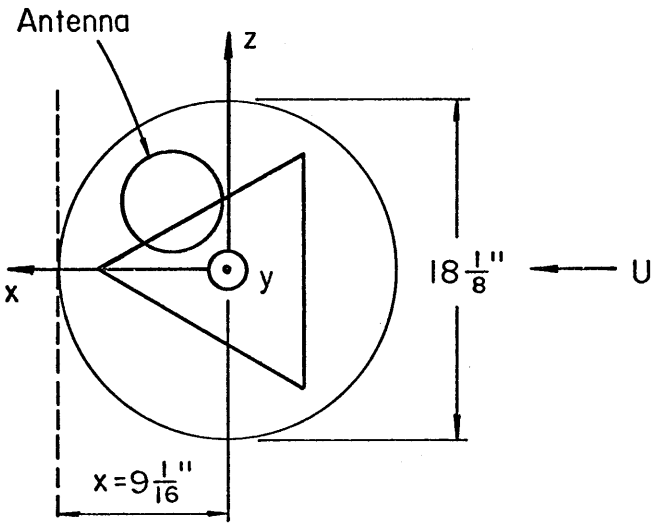

POSITION 2

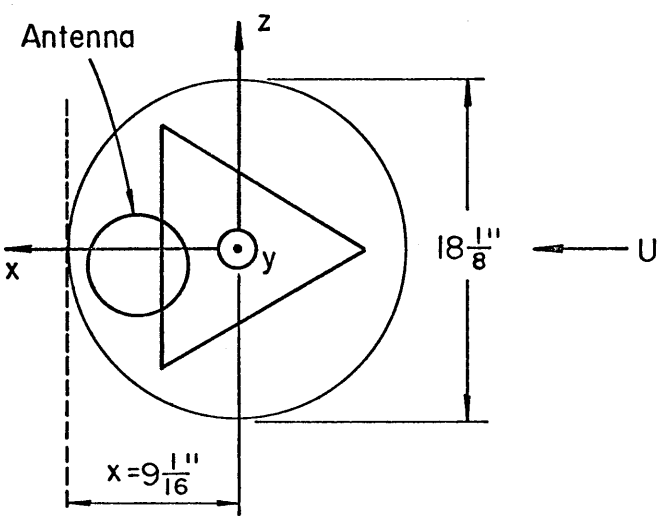

Fig. 4. The model positions with antenna's dish horizontal.

POSITION 1

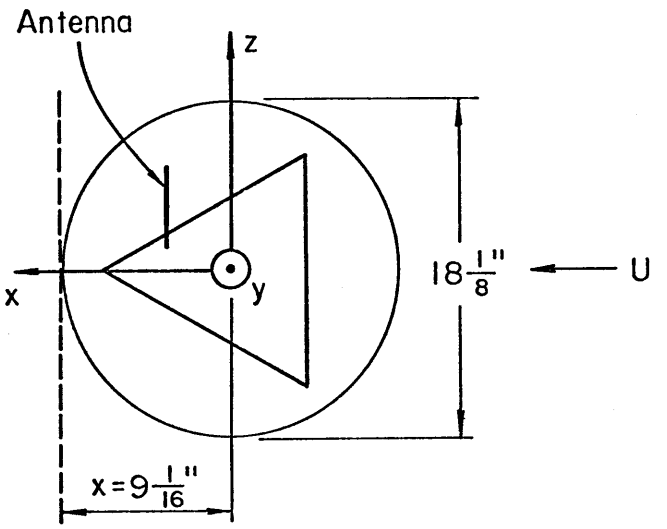

POSITION 2

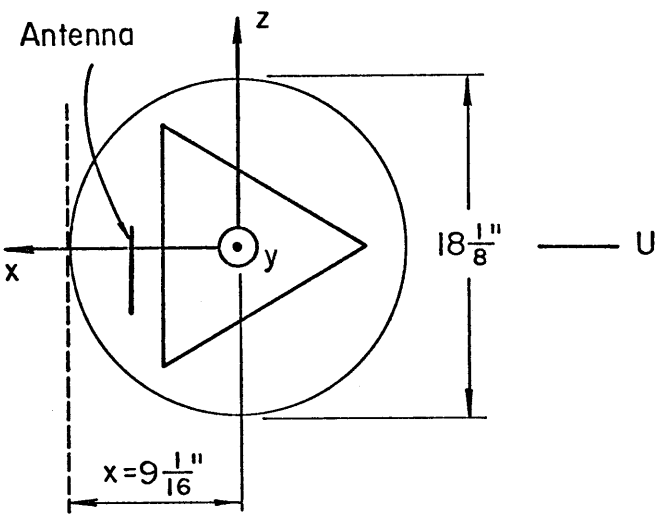

Fig. 5. The model positions with antenna's dish vertical.

Vertical Survey:
Antenna Vertical

Position 1

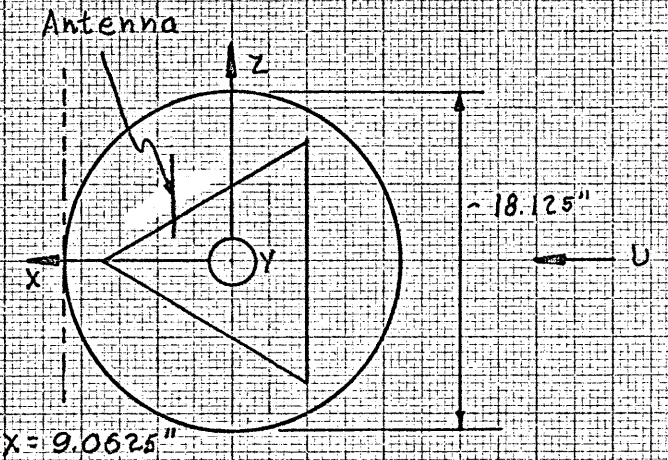

Position 2

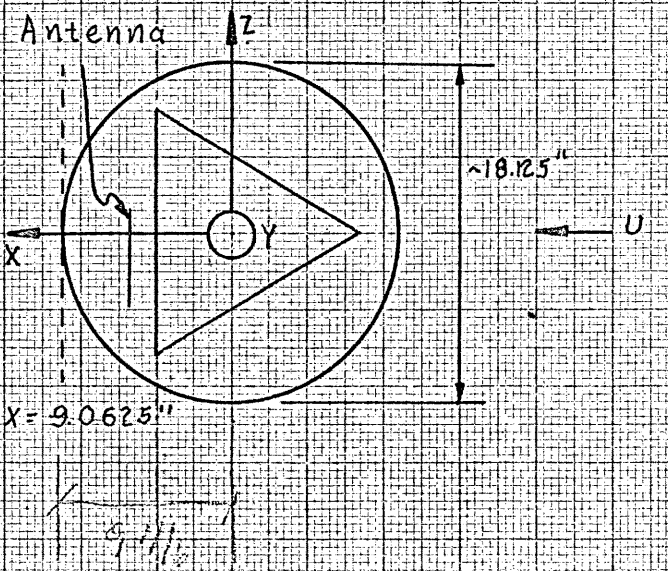

ADDENDUM

(Section 3.4)

A PRELIMINARY STUDY OF FLOW FIELD ABOUT VIKING LANDER MODEL

by

W. Z. Sadeh and V. A. Sandborn

October 1970 CER70-71WZS-VAS-18

3.4 Velocity Defect Thin-Thick Boundary Layer, Position 1 and 2, High Velocity, Dish Horizontal; (A-B)-HV-DH-1 or 2

In order to obtain a better evaluation of the shear flow effect on velocity distribution the combined normalized defect law, i.e., $(1 - \frac{U_1}{U_o}\frac{U_{o\delta}}{U_{1\delta}})_B - (1 - \frac{U_1}{U_o}\frac{U_{o\delta}}{U_{1\delta}})_A$ based on the thin and thick boundary layer normalized defect laws, respectively, was calculated. The results at $z = 0, \pm 7$ and ± 14 in in plane $x = 9\ 1/16$ in are displayed in Figs. (A-B)-HV-DH-1-VS and (A-B)-HV-DH-2-VS.

Generally, the normalized defect is relatively small except at a few particular locations. Furthermore, a lesser defect is observed in position 2 than in position 1. The larger defect was monitored for both positions at $z = 0$. In addition, in position 1, at $z = -7$ in a relatively strong defect is observed at $y = 1$ and 4 in. In position 2, the defect is roughly 4 times smaller at $y = 1$ in whereas no defect was monitored at $y = 4$ in.

The results indicate that velocity distribution is slightly affected by the shear flow except at several particular locations. The effect is quite small but, nevertheless, it is important to evaluate it. The normalized defect law can be used to estimate the boundary layer effect,

LIST OF FIGURES SUBMITTED

Figure	Description	Position (in)	No. of Figures
(A-B)-HV-DH-1-VS	$(1-\frac{U_1}{U_o}\frac{U_{o\delta}}{U_{1\delta}})_B - (1-\frac{U_1}{U_o}\frac{U_{o\delta}}{U_{1\delta}})_A$ vs. y	z=0,±7,±14	2
(A-B)-HV-DH-2-VS	$(1-\frac{U_2}{U_o}\frac{U_{o\delta}}{U_{2\delta}})_B - (1-\frac{U_2}{U_o}\frac{U_{o\delta}}{U_{2\delta}})_A$ vs. y	z=0,±7,±14	2
B-HV-DH-1-VS	$(1-\frac{U_1}{U_o}\frac{U_{o\delta}}{U_{1\delta}})_B$ vs. y	z=0,±7,±14	1
B-HV-DH-2-VS	$(1-\frac{U_2}{U_o}\frac{U_{o\delta}}{U_{2\delta}})_B$ vs. y	z=0,±7,±14	1